Proceedings of ASME Turbo Expo 2011
GT2011
June 6-10, 2011, Vancouver, British Columbia, Canada

GT2011-46367

SIMULATION OF UNSTEADY TURBOMACHINERY FLOWS USING AN IMPLICITLY COUPLED NONLINEAR HARMONIC BALANCE METHOD

Jonathan M. Weiss*
Venkataramanan Subramanian
CD-adapco
Lebanon, New Hampshire, 03766
Email: jonathan.weiss@us.cd-adapco.com

Kenneth C. Hall
Department of Mechanical Engineering and Materials Science
Duke University
Durham, North Carolina, 27708

ABSTRACT

A nonlinear harmonic balance method for the simulation of turbomachinery flows is presented. The method is based on representing an unsteady, time periodic flow by a Fourier series in time and then solving a set of mathematically steady-state equations to obtain the Fourier coefficients. The steady-state solutions are stored at discrete time levels distributed throughout one period of unsteadiness and are coupled via the physical time derivative and at periodic boundaries. Implicit coupling between time levels is achieved in a computationally efficient manner through approximate factorization of the linear system that results from the discretized equations.

Unsteady, rotor-stator interactions are performed to validate the implementation. Results based on the harmonic balance method are compared against those obtained using a full unsteady, time-accurate calculation using moving meshes. The implicitly coupled nonlinear harmonic balance method is shown to produce a solution of reasonable accuracy compared to the full unsteady approach but with significantly less computational cost.

INTRODUCTION

As the use of Computational Fluid Dynamics (CFD) becomes a regular part of the design cycle, concerns arise regarding the computational cost and turn-around time associated with employing CFD for the simulation and analyses of unsteady flows in turbomachines, especially for multistage machines with unequal blade counts.

Full unsteady simulations that integrate the governing equations in time can be performed to model the nonlinear unsteady disturbances by marching time accurately from one physical time instant to the next. The flowfields within multiple blade rows are solved simultaneously and the meshes within adjacent rows are moved relative to one another with each time step. However, the computational expense of this approach can be significant. This is because sub-iterations are required at each time instant, the time step size is necessarily small to preserve time accuracy, and many time steps are required to reach a time periodic solution. Additionally, multiple passages must be meshed to achieve spatial periodicity, unless so-called phase-lagged boundary conditions [1, 2] are used to reduce the size of the computational domain to a single blade passage in each blade row.

Alternatively, given the time periodic nature of these flows, one can model the unsteady flow in turbomachines using nonlinear, harmonic balance techniques. Roughly speaking, the family of nonlinear harmonic methods expands the unsteady flow field in a Fourier series in time and solves for the Fourier coefficients. He [3], He and Ning [4] and Ning and He [5] developed a harmonic method in which the unsteady harmonics are treated as perturbations. Hall, Thomas, and Clark [6] developed a full harmonic balance method, which allows for arbitrarily large disturbances and any number of harmonics. The method is computationally efficient and stores the unsteady nonlinear solutions as the working variables at several time levels over one period of unsteadiness, rather than storing the Fourier coefficients them-

*Address all correspondence to this author.

Copyright © 2011 by ASME

selves. Gopinath and Jameson [7] and others have applied this approach to turbomachinery applications. McMullen, Jameson, and Alonso [8] and others have developed a similar approach, but store as the working variables the Fourier coefficients and convert the solution from the frequency to the time domain in order to compute the spatial residual. For an excellent recent survey of Fourier methods applied to turbomachinery applications, see the survey paper by He [9].

In all these methods, the harmonic balance equations are solved by introducing a pseudo-time derivative term and then marching the coupled equations to a steady state in pseudo-time using an explicit time marching method such as Lax-Wendroff or Runge-Kutta. Recently, Custer et al [10] implemented the harmonic balance method in an existing structured grid overset Navier-Stokes flow solver and employed point-wise implicit treatment of the harmonic balance source term to provide numerical stability. Woodgate and Badcock [11] developed an implicit harmonic balance method using approximate Jacobians and a Krylov-type sparse matrix solver.

In this paper we describe an implicitly coupled, nonlinear harmonic balance method in which the unsteady flowfield is represented by a Fourier series in time. The Fourier coefficients are obtained by simultaneously solving a set of harmonic balance equations written in terms of the unsteady, nonlinear solution variables stored at discrete time levels distributed throughout a single period of unsteadiness. The number of time levels required is determined by the desired number of harmonics retained in the model. For a single stage (rotor and stator) the frequencies associated with the Fourier series are integer multiples of the fundamental excitation frequency (e.g. the blade passing frequency). For three or more blade rows the frequency content is slightly more complicated, but still remains a function of the blade counts and rotor speed.

We approximate the physical time derivative by a pseudo-spectral operator such that the resultant fluid dynamic equations describing each time level are effectively steady-state. However, the solutions at each time level remain coupled to one another at the periodic boundaries and through the physical time derivative. To accommodate implicit solution of the dependent variables at all time levels, an approximate factorization is used to split the resultant linearized system to yield two implicit operators. The first operator, which is decoupled across the time levels, contains a full linearization of the spatially discretized fluxes at a given time level with respect to the variables at that time level. The second operator, which couples the time levels at a given point, contains the linearization of the physical time derivative with respect to the variables at all levels. Provisional solutions are obtained by sequentially applying the first operator to each time level and solving the resultant system by means of a coupled, algebraic multigrid method [12]. Then the second operator is applied simultaneously to the provisional solutions at all time levels to obtain the final solution for the iteration.

A cell-centered, polyhedral-based, finite-volume discretization of the governing equations is used in conjunction with flux-difference splitting [13] and a linear reconstruction of variables [14]. At inter-row boundaries, selected Fourier coefficients are matched based upon the flowfield kinematics [15]. Unsteady, non-reflecting boundary conditions [16, 17] are applied to the remaining set of coefficients, and at the farfield boundaries as well.

Results of unsteady, rotor-stator interactions are presented to validate our implementation of an implicitly coupled harmonic balance method. These results are compared against those obtained using a full unsteady, time-accurate calculation performed on moving meshes. We show that the harmonic balance method can produce a solution of reasonable accuracy compared to the full unsteady approach with significantly less computational cost.

GOVERNING EQUATIONS

Consider the Navier-Stokes equations in integral form for a rigid, arbitrary control volume V with differential surface area $d\vec{A}$ in a relative frame of reference rotating steadily with angular velocity $\boldsymbol{\Omega}$:

$$\int_V \frac{\partial \boldsymbol{W}}{\partial t}\, dV + \oint \left[\vec{\boldsymbol{F}} - \vec{\boldsymbol{G}}\right] \cdot d\vec{A} = \int_V \boldsymbol{S}\, dV \tag{1}$$

where $\boldsymbol{W}$ is the solution vector of conservation variables

$$\boldsymbol{W} = [\rho, \rho\boldsymbol{u}, \rho E]^T$$

$\vec{\boldsymbol{F}}$, $\vec{\boldsymbol{G}}$ and $\boldsymbol{S}$ are the inviscid flux, viscous flux, and source vectors

$$\begin{aligned}
\vec{\boldsymbol{F}} &= \left[\rho\boldsymbol{v}, \rho\boldsymbol{u}\otimes\boldsymbol{v} + p\bar{\bar{I}}, \rho E\boldsymbol{v} + p\boldsymbol{u}\right]^T \\
\vec{\boldsymbol{G}} &= [0, \bar{\bar{\boldsymbol{\tau}}}, \bar{\bar{\boldsymbol{\tau}}}\cdot\boldsymbol{v} + \boldsymbol{q}]^T \\
\boldsymbol{S} &= [0, \rho\,\boldsymbol{\Omega}\otimes\boldsymbol{u}, 0]^T
\end{aligned}$$

Here ρ, $\boldsymbol{u}$, E, and p are the density, absolute velocity, total enthalpy, and pressure, respectively. $\boldsymbol{v}$ is the relative velocity, $\boldsymbol{v} = \boldsymbol{u} - \boldsymbol{r}\otimes\boldsymbol{\Omega}$

Harmonic Balance Equations

Since the solution $\boldsymbol{W}$ is periodic in time, we can represent it by the Fourier series:

$$\boldsymbol{W}(\vec{\boldsymbol{x}}, t) = \sum_{m=-M}^{M} \hat{\boldsymbol{W}}_m(\vec{\boldsymbol{x}})\, e^{i\omega m t} \tag{2}$$

Copyright © 2011 by ASME

where ω is the fundamental frequency of the disturbance, M is the number of harmonics retained in the solution, and $\hat{\boldsymbol{W}}_m$ are the Fourier coefficients. The coefficients $\hat{\boldsymbol{W}}_m$ can be uniquely determined from the discrete Fourier transform:

$$\hat{\boldsymbol{W}}_m(\vec{\boldsymbol{x}}) = \frac{1}{N}\sum_{n=0}^{N-1} \boldsymbol{W}_n^*(\vec{\boldsymbol{x}}, t_n)\, e^{-i\omega m t_n} \tag{3}$$

where $\boldsymbol{W}_n^*$ are a set of $N = 2M + 1$ solutions at discrete time levels $t_n = nT/N$ distributed throughout one period of unsteadiness, T.

At any location in the flowfield domain we can transform the time level solutions into Fourier coefficients and vice versa using a discrete Fourier transform operator E and its corresponding inverse E^{-1} as follows

$$\hat{\boldsymbol{W}} = \mathrm{E}\,\boldsymbol{W}^* \tag{4}$$

$$\boldsymbol{W}^* = \mathrm{E}^{-1}\,\hat{\boldsymbol{W}} \tag{5}$$

where E and E^{-1} are square matrices of dimension $N \times N$, and the Fourier coefficients and time level solutions have been assembled into the vectors $\hat{\boldsymbol{W}}$ and $\boldsymbol{W}^*$, respectively

$$\hat{\boldsymbol{W}} = \left[\hat{\boldsymbol{W}}_{-M}, \hat{\boldsymbol{W}}_{-M+1}, \cdots, \hat{\boldsymbol{W}}_{M-1}, \hat{\boldsymbol{W}}_M\right]^T$$

$$\boldsymbol{W}^* = \left[\boldsymbol{W}_0^*, \boldsymbol{W}_1^*, \cdots, \boldsymbol{W}_{N-2}^*, \boldsymbol{W}_{N-1}^*\right]^T$$

The solutions at each discrete time level are obtained by applying the governing equations, Eqn. (1), to all the $\boldsymbol{W}^*$ simultaneously

$$\int_V \frac{\partial \boldsymbol{W}^*}{\partial t}\, dV + \oint \left[\vec{\boldsymbol{F}}^* - \vec{\boldsymbol{G}}^*\right] \cdot d\vec{A} = \int_V \boldsymbol{S}^*\, dV \tag{6}$$

where the flux and source vectors $\vec{\boldsymbol{F}}^*$, $\vec{\boldsymbol{G}}^*$ and $\boldsymbol{S}^*$ are evaluated using the corresponding time level solution, for example

$$\vec{\boldsymbol{F}}^* = \left[\vec{\boldsymbol{F}}(\boldsymbol{W}_0^*), \vec{\boldsymbol{F}}(\boldsymbol{W}_1^*), \cdots, \vec{\boldsymbol{F}}(\boldsymbol{W}_{N-2}^*), \vec{\boldsymbol{F}}(\boldsymbol{W}_{N-1}^*)\right]^T$$

The time derivative in Eqn. (6) is evaluated by differentiating Eqn. (5) with respect to time and then employing Eqn. (4) as follows:

$$\frac{\partial \boldsymbol{W}^*}{\partial t} = \frac{\partial \mathrm{E}^{-1}}{\partial t}\,\hat{\boldsymbol{W}} = \frac{\partial \mathrm{E}^{-1}}{\partial t}\,\mathrm{E}\,\boldsymbol{W}^*$$

or

$$\frac{\partial \boldsymbol{W}^*}{\partial t} = \mathrm{D}\,\boldsymbol{W}^* \tag{7}$$

where D is the pseudo-spectral, $N \times N$ matrix operator. Substituting Eqn. (7) for the time derivative in Eqn. (6) yields the desired harmonic balance equations

$$\int_V \mathrm{D}\,\boldsymbol{W}^*\, dV + \oint \left[\vec{\boldsymbol{F}}^* - \vec{\boldsymbol{G}}^*\right] \cdot d\vec{A} = \int_V \boldsymbol{S}^*\, dV \tag{8}$$

BOUNDARY CONDITIONS

To motivate the presentation of boundary conditions we first consider the flowfield kinematics of two adjacent blade rows where the first row has B_1 blades spinning with rotational rate Ω_1 rad/s and the second has B_2 blades spinning with rotational rate Ω_2 rad/s. The flowfield within the stage can be decomposed into a Fourier series in the rotational direction characterized by a set of N_{m_1,m_2} nodal diameters

$$N_{m_1,m_2} = m_1 B_1 + m_2 B_2 \tag{9}$$

where m_1 and m_2 can take on all integer values. In the frame of reference of the first blade row, the frequency of the unsteady disturbance associated with any nodal diameter is

$$\omega_{1,m_2} = m_2 B_2 (\Omega_1 - \Omega_2)$$

while in the frame of reference of the second row, the frequencies are

$$\omega_{m_1,2} = m_1 B_1 (\Omega_2 - \Omega_1)$$

Note that in either row the unsteady frequency associated with a given nodal diameter is a function of the blade count and relative rotation rate of the adjacent row. Furthermore, associated with each unsteady frequency is an interblade phase angle

$$\sigma_{1,m_2} = m_2\, 2\pi \frac{B_2}{B_1}$$

in the frame of reference of the first blade row, and

$$\sigma_{m_1,2} = m_1\, 2\pi \frac{B_1}{B_2}$$

Copyright © 2011 by ASME

in the frame of reference of the second row. Clearly the interblade phase angles associated with a given nodal diameter are a function of the pitch ratios between the two rows. Note that the pitch in each row is given by $G_1 = 2\pi/B_1$ and $G_2 = 2\pi/B_2$ in the first and second rows, respectively.

Periodic Boundaries

We apply complex periodicity conditions at the periodic boundaries in the rotational direction. This allows us to reduce the computational domain to a single passage in each row, thereby decreasing significantly the size and cost of the computation, particularly in the case of unequal blade counts. Consider $\boldsymbol{W}(r,\theta,z,t)$ and $\boldsymbol{W}(r,\theta+G,z,t)$ to represent the solution on the lower and upper periodic boundaries in cylindrical space and at time t, where θ is the rotational direction and G the blade pitch. Spatial periodicity requires that

$$\boldsymbol{W}(r,\theta+G,z,t) = \boldsymbol{W}(r,\theta,z,t+\Delta T) \tag{10}$$

where ΔT is the time lag associated with the interblade phase angle. Considering Eqn. (2), we can express the time shift implied by Eqn. (10) in terms of the Fourier coefficients $\hat{\boldsymbol{W}}$ as

$$\hat{\boldsymbol{W}}(r,\theta+G,z) = \hat{\boldsymbol{W}}(r,\theta,z)\, e^{i\sigma/\omega} \tag{11}$$

where we have used the relation $\Delta T = \sigma/\omega$. In our example of two blade rows, the time lag in each row is given by $\Delta T_1 = \sigma_{1,m_2}/\omega_{1,m_2} = 2\pi/(B_1(\Omega_1-\Omega_2))$ and $\Delta T_2 = \sigma_{m_1,2}/\omega_{m_1,2} = 2\pi/(B_2(\Omega_2-\Omega_1))$ in the first and second rows, respectively.

Hence the procedure of applying the periodic boundary condition to the solution at any given time level involves first computing the temporal Fourier coefficients using all the $\boldsymbol{W}^*$ by means of Eqn. (4) and applying the phase shift to the resultant $\hat{\boldsymbol{W}}$ as given by Eqn. (11). These are then transformed back to the time domain by means of Eqn. (5) to yield phase-shifted solutions at all time levels. The resultant phase-shifted solution at the given time level is then used to satisfy Eqn. (10). Thus the solutions at all time levels become coupled to one another through the periodic boundary conditions.

Farfield Boundaries

Non-reflecting, farfield boundary conditions are applied at the inflow and outflow boundaries of the domain. This treatment prevents spurious unsteady numerical disturbances from reflecting back into the computational domain and corrupting the solution. It also permits the use of truncated computational domains, with boundaries positioned near to the leading and trailing edges of the outermost blade rows, to further reduce the size and cost of the computation.

The procedure begins by computing the temporal Fourier coefficients $\hat{\boldsymbol{W}}$ at all points along the boundary. These are then decomposed further by means of the following discrete, spatial Fourier transform in the rotational, or circumferential, direction

$$\hat{\hat{\boldsymbol{W}}}(r,z)_{m_1,m_2} = \frac{1}{G}\sum_{j=0}^{Np-1} \hat{\boldsymbol{W}}(r,\theta_j,z)\, e^{-iN_{m_1,m_2}\theta_j}\, d\theta_j \tag{12}$$

where Np is the number of discrete points in that direction and N_{m_1,m_2} is the nodal diameter given by Eqn. (9). Given the example of two blade rows, at the inlet to the first row we let m_1 be all the spatial circumferential modes supported by the mesh and m_2 be all the temporal modes retained in the solution in that row, while at the exit of the second row we let m_1 be all the temporal modes and m_2 the maximum number of spatial circumferential modes allowed by the mesh resolution.

Given the set of Fourier coefficients $\hat{\hat{\boldsymbol{W}}}_{m_1,m_2}$ we modify those defining the mean flow, i.e. for which $m_1 = m_2 = 0$, in a manner similar to that described by Saxer [18] to enforce conventional steady flow boundary conditions. Total pressure, total temperature and flow angle of the mean flow are specified at the inflow boundary and the static pressure of the mean flow is specified at the outflow boundary. The remaining coefficients with $m_1 \neq m_2 \neq 0$ are modified to eliminate unwanted reflected waves. This is accomplished by performing an eigenmode analysis to determine the direction and speed of propagation of the eigenvalues associated with each coefficient and then setting to zero those waves traveling back into the domain [16,17]. Finally, the modified Fourier coefficients are inversely transformed, both spatially and temporally, to produce updated solutions at all time levels on the inflow and outflow boundaries. Like at periodic boundaries, the time level solutions are coupled to one another through the non-reflecting farfield boundary conditions as well.

Inter-Row Boundaries

At each iteration of the harmonic balance scheme the solutions at all discrete time levels and in all blade rows are solved, following which inter-row conditions are applied at the interface boundaries between rows in order to achieve multistage coupling. This procedure follows closely that described above for farfield boundaries. First, two sets of Fourier coefficients, one set corresponding to the solution on each of the two boundaries composing the interface, are computed by means of Eqn. (12). Then coefficients from each set with the same nodal diameter (see Eqn. (9)) are set equal to one another, while the remaining coefficients are treated by the same non-reflecting procedure employed at the farfield boundary. Finally, the modified Fourier coefficients are transformed back in time and space to yield updated solutions on the inter-row boundaries. Again, this procedure has the effect of coupling all the time level solutions.

Copyright © 2011 by ASME

SOLUTION PROCEDURE

The harmonic balance equations are discretized using a cell-centered, polyhedral-based, finite-volume scheme. Second order spatial accuracy is achieved by means of a multi-dimensional, linear reconstruction of the solution variables [14]. The convective fluxes are evaluated by a standard upwind, flux-difference splitting [13] and the diffusive fluxes by a second-order central difference. A pseudo-time derivative of primitive quantities, $\partial \boldsymbol{Q}/\partial\tau$, with $\boldsymbol{Q} = \{p, \boldsymbol{u}, T\}$, is introduced into Eqn. (8) to facilitate solution of the steady harmonic balance equations by means of a time marching procedure. An Euler implicit discretization in pseudo-time [19] produces the following linearized system of equations:

$$\left[\frac{\partial \boldsymbol{W}}{\partial \boldsymbol{Q}} + \Delta\tau\left(\mathrm{A} - \frac{\partial \boldsymbol{S}}{\partial \boldsymbol{Q}} + \mathrm{D}\,\frac{\partial \boldsymbol{W}}{\partial \boldsymbol{Q}}\right)\right]\Delta\boldsymbol{Q}^* = -\Delta\tau\boldsymbol{R}^* \quad (13)$$

where $\boldsymbol{R}^*$ is the discrete residual of Eqn. (8), and $\Delta\boldsymbol{Q}^*$ are the resultant primitive variable corrections across one pseudo-time step, $\Delta\tau$. Operator A is the Jacobian of the discrete inviscid and viscous flux vectors with respect to primitive variables $\boldsymbol{Q}$ and introduces both center coefficients as well as off-diagonals arising from the linearization of the spatially discretized fluxes.

The coupled system given by Eqn. (13) contains equations from all time levels linked at every point in the domain by the pseudo-spectral operator D. The result is is a large system, and solving it all at once would be rather intractable. However, we can exploit the point coupled nature of the system and employ approximate factorization to produce the following two step scheme:

$$\left[\frac{\partial \boldsymbol{W}}{\partial \boldsymbol{Q}} + \Delta\tau\left(\mathrm{A} - \frac{\partial \boldsymbol{S}}{\partial \boldsymbol{Q}}\right)\right]\Delta\tilde{\boldsymbol{Q}}^* = -\Delta\tau\boldsymbol{R}^* \quad (14)$$

$$\left[\bar{\bar{I}} + \Delta\tau\,\frac{\partial \boldsymbol{W}}{\partial \boldsymbol{Q}}^{-1}\mathrm{D}\,\frac{\partial \boldsymbol{W}}{\partial \boldsymbol{Q}}\right]\Delta\boldsymbol{Q}^* = \Delta\tilde{\boldsymbol{Q}}^* \quad (15)$$

where $\Delta\tilde{\boldsymbol{Q}}^*$ represents provisional corrections to the solution.

In the first step, Eqn. (14), the time levels are no longer coupled and we can solve for the $\Delta\tilde{\boldsymbol{Q}}^*$ one time level at a time. With the exception of the physical time derivative appearing in Eqn. (8), the evaluation of fluxes, accumulation of the residual, and the process of assembling and solving Eqn. (14) at each time level proceeds exactly as for a single, steady-state solution in the time domain. Here we employ an algebraic multigrid (AMG) method to solve the linear system (Eqn. (14)) and obtain the provisional $\Delta\tilde{\boldsymbol{Q}}^*$. In the second step the complete corrections $\Delta\boldsymbol{Q}^*$ for the current iteration are obtained by inverting Eqn. (15) at each point in the domain given all the $\Delta\tilde{\boldsymbol{Q}}^*$ computed in step one.

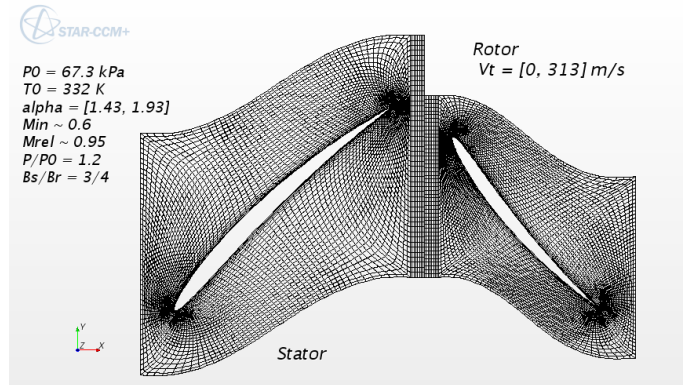

FIGURE 1. COMPUTATIONAL MESH FOR TWO-DIMENSIONAL COMPRESSOR STAGE.

RESULTS

In this section we compare results obtained from the implicitly coupled, non-linear harmonic balance method described above with solutions from a full, unsteady simulation based on the standard dual time-stepping approach. The test case consists of a model two-dimensional compressor stage; specifically, the first stator and second rotor rows of the five row, "Configuration D" described by Ekici and Hall [20]. A representative computational mesh for this problem is shown in Fig. 1. There are three stator blades to every four rotor blades. The two blade rows are separated by an axial gap equal to 0.25 times the aerodynamic chord of the rotor. The Mach number at the inlet to the stator is 0.68 and the relative Mach number entering the rotor is 0.71. The static-to-total pressure ratio across the stage is 1.2.

Three separate Euler calculations are made using the non-linear harmonic balance method in which one, two and three harmonics, respectively, are retained for the blade passing frequencies in both the stator and rotor. Contours of instantaneous pressure, representative of the flow field within the compressor stage and computed using three harmonics in each blade row, are shown in Fig. 2. Note that computations are performed on just the center blade passage outlined in each row. The solutions shown in the passages above and below are phase-shifted reconstructions included for clarity. The convergence history for the case with three harmonics (seven time levels) is shown in Fig. 3 which shows the L2-norm of $\boldsymbol{R}^*$, the discrete residual of Eqn. (8) assembled over all time levels, plotted vs. iteration. The convergence rate shown is typical of each of the three calculations. Convergence is achieved in about 4000 iterations. On a Linux workstation (Intel® Xeon® CPU X5570@2.93GHz (x86_64)) these calculations took 1200, 2320, and 3320 seconds of CPU time for the one, two and three harmonic cases, respectively.

By way of comparison, the unsteady, dual time-stepping solver is run on a domain consisting of three stator passages and

Copyright © 2011 by ASME

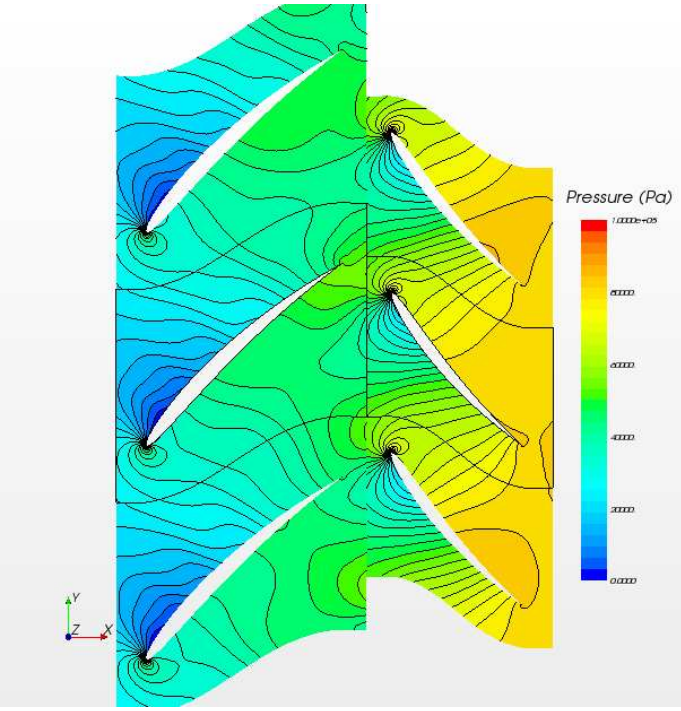

FIGURE 2. INSTANTANEOUS PRESSURE DISTRIBUTION WITHIN THE COMPRESSOR STAGE COMPUTED USING NONLINEAR HARMONIC BALANCE METHOD.

four rotor passages in order to satisfy the spatial periodicity requirement. The physical time step size is set such that the rotor advances across one grid cell on the stator outlet boundary per time step. This produces 36 and 48 time steps per period in the stator and rotor, respectively. Twenty iterations are run per time step. The unsteady simulation is continued for about 100 rotor periods (4800 time steps) until time-periodic behavior is achieved. The CPU time required is 0.73 seconds per iteration or about 15 seconds per time step, for a total of approximately 20 hours. This is compared to less than one hour of CPU time for the harmonic balance calculation retaining three harmonics (seven time levels). Once a time-periodic, unsteady solution is obtained a discrete Fourier transform (DFT) is applied to the final 36 and 48 time step solutions in the stator and rotor, respectively, and the resultant Fourier coefficients are compared with those obtained by means of the nonlinear harmonic balance method.

The predicted mean pressure loadings on the stator and rotor from the three harmonic balance simulations are compared against the time averaged solution from the unsteady run and a steady solution based on a mixing-plane approach in Figs. 4 and 5, respectively. That is, we use the present harmonic balance solver, but with zero harmonics, to compute the steady flow through the two blade rows. These results show nearly the same time mean solution is predicted in all instances, but with small

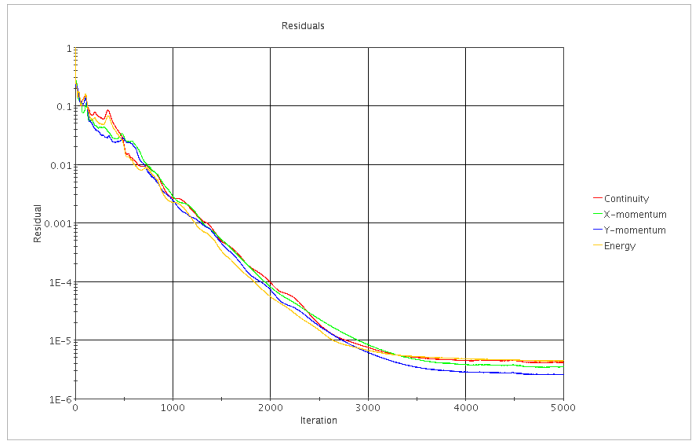

FIGURE 3. RESIDUAL HISTORY FOR COMPRESSOR STAGE CALCULATION USING NONLINEAR HARMONIC BALANCE METHOD.

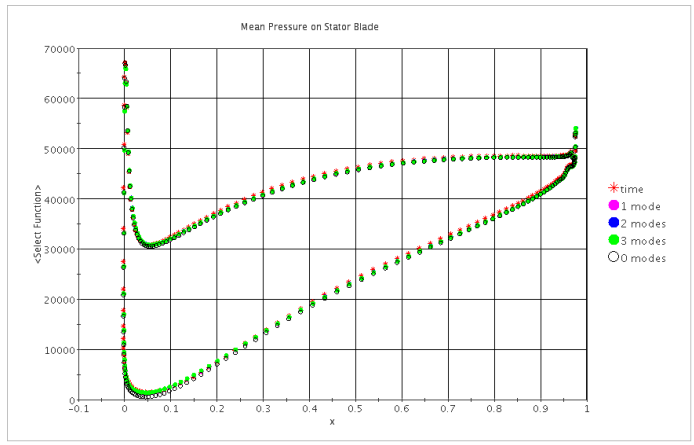

FIGURE 4. MEAN PRESSURE DISTRIBUTION ON THE STATOR.

differences seen between the steady mixing plane (zero harmonics) solution. These small differences are likely due to nonlinear effects, which for this example are small.

In Fig. 6 we compare the magnitude of the first mode of the unsteady pressure on the stator as predicted by the three harmonic balance runs against that given by the DFT of the unsteady simulation. Similar comparison of the phase of the first mode of the unsteady pressure on the stator is shown in Fig. 7. These results show very reasonable agreement between the harmonic balance and time domain solutions. Note that the magnitude of the unsteady pressure is about 10% of the mean value and the spread between the harmonic balance results obtained when retaining one, two, or three harmonics is only about 2% of the mean. This suggests that reasonable results can be obtained given just a few

Copyright © 2011 by ASME

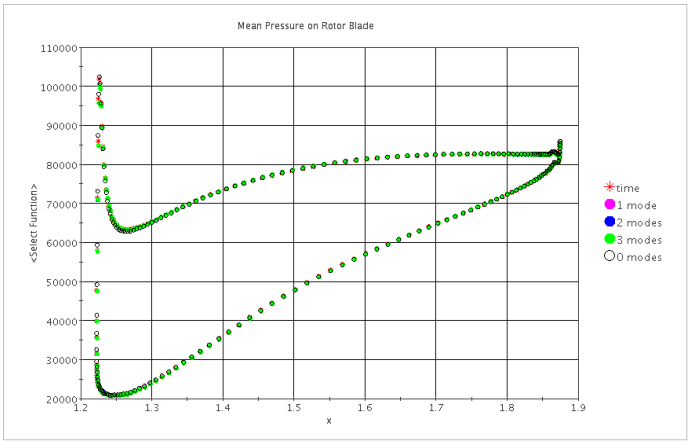

FIGURE 5. MEAN PRESSURE DISTRIBUTION ON THE ROTOR.

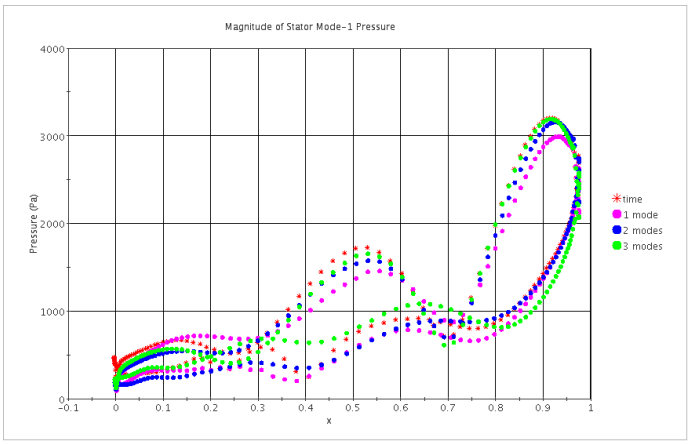

FIGURE 6. MAGNITUDE OF THE 1st MODE OF UNSTEADY PRESSURE ON THE STATOR.

harmonics of the fundamental frequencies.

Figures 8 and 9 show comparisons of the magnitude and phase, respectively, of the first mode of the unsteady pressure on the rotor. Again, the harmonic balance shows reasonable agreement with the time domain. However, here in the rotor we do see more variation amongst the predictions, particularly near the trailing edge.

SUMMARY

In this paper we have presented the development of an implicitly coupled nonlinear harmonic balance method for the solution of time periodic flows in turbomachines. The advantage of the current method is that it is based on solving a set of steady-state equations in the time-domain which allows for the reuse of existing steady-state implementations. Furthermore, the implicit

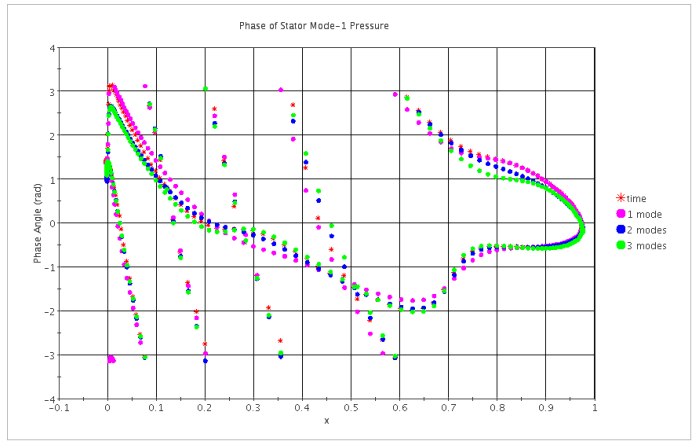

FIGURE 7. PHASE OF THE 1st MODE OF UNSTEADY PRESSURE ON THE STATOR.

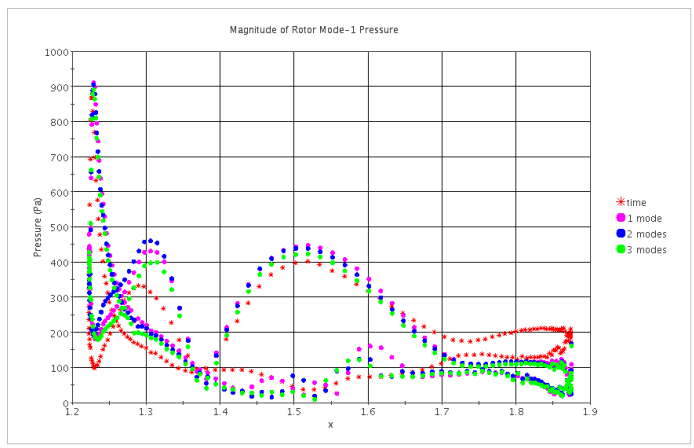

FIGURE 8. MAGNITUDE OF THE 1st MODE OF UNSTEADY PRESSURE ON THE ROTOR.

coupling maintained between time levels results in an efficient and stable algorithm.

The harmonic balance method described was applied to a test case consisting of a model two-dimensional compressor stage. Results were obtained for runs retaining one, two and three harmonics of the blade passing frequencies in both the stator and rotor. Three results compared reasonably with those obtained by means of a full unsteady, time-accurate calculation performed on moving meshes, in terms of both mean flow predictions as well as predicted magnitude and phase of the first mode of the unsteady pressure. It was also shown that reasonable accuracy can be achieved by retaining as few as two or three harmonics of the fundamental frequency.

Copyright © 2011 by ASME

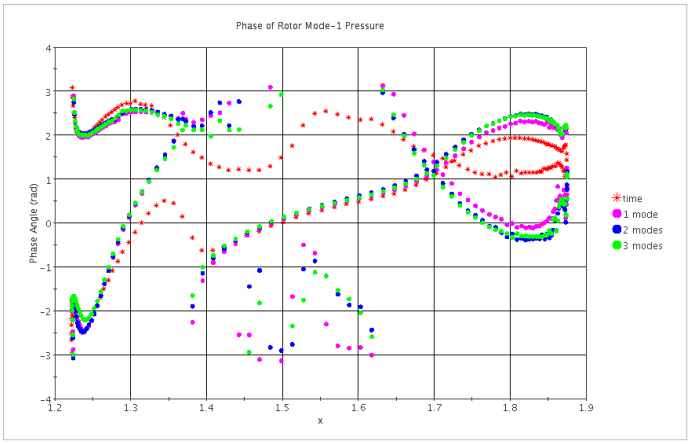

FIGURE 9. PHASE OF THE 1st MODE OF UNSTEADY PRESSURE ON THE ROTOR.

REFERENCES

[1] Dewhurst, S., and He, L., 2000. "Unsteady flow calculations through turbomachinery stages using single-passage domain with shape-correction method". In Proceedings of the 9th International Symposium on Unsteady Aerodynamics, Aeroacoustics, and Aeroelasticity in Turbomachines, P. Ferrand and S. Aubert, eds.

[2] Schnell, R., 2004. Investigation of the Tonal Acoustic Field of a Transonic Fan Stage by Time-Domain CFD-Calculations with Arbitrary Blade Counts. ASME Paper GT2004-54216.

[3] He, L., 1996. "Modelling issues for time-marching calculations of unsteady flows, blade row interaction and blade flutter". In *VKI Lecture Series "Unsteady Flows in Turbomachines"*. von Karman Institute for Fluid Dynamics.

[4] Ning, W., and He, L., 1998. "Computation of Unsteady Flows Around Oscillating Blades Using Linear and Non-Linear Harmonic Euler Methods". *Journal of Turbomachinery*, ***120***(3), pp. 508–514.

[5] He, L., and Ning, W., 1998. "Efficient approach for analysis of unsteady viscous flows in turbomachines". *AIAA Journal*, ***36***(11), pp. 2005–2012.

[6] Hall, K. C., Thomas, J. P., and Clark, W. S., 2002. "Computation of Unsteady Nonlinear Flows in Cascades Using a Harmonic Balance Technique". *AIAA Journal*, ***40***(5), May, pp. 879–886.

[7] Gopinath, A., and Jameson, A., 2005. Time Spectral Method for Periodic Unsteady Computations over Two- and Three- Dimensional Bodies. AIAA Paper 2005-1220.

[8] McMullen, M., Jameson, A., and Alonso, J., 2001. Acceleration of Convergence to a Periodic Steady State in Turbomachinery Flows. AIAA Paper 2001-0152.

[9] He, L., 2010. "Fourier methods for turbomachinery applications". *Progress in Aerospace Sciences*, ***46***(8), pp. 329 – 341.

[10] Thomas, J., Custer, C., Dowell, E., and Hall, K., 2009. Unsteady Flow Computation Using a Harmonic Balance Approach Implemented about the OVERFLOW 2 Flow Solver. AIAA Paper 2009-427.

[11] Woodgate, M., and Badcock, K., 2009. "Implicit Harmonic Balance Solver for Transonic Flow with Forced Motions". *AIAA Journal*, ***47***(4), Apr., pp. 893–901.

[12] Ruge, J. W., and Stuben, K., 1987. "Algebraic Multigrid". In *Multigrid Methods*, S. F. McCormick, ed. SIAM.

[13] Roe, P. L., 1986. "Characteristic Based Schemes for the Euler Equations". *Annual Review of Fluid Mechanics*, ***18***, pp. 337–365.

[14] Barth, T. J., and Jespersen, D. C., 1989. The Design and Application of Upwind Schemes on Unstructured Meshes. AIAA Paper 89-0366.

[15] Ekici, K., and Hall, K. C., 2006. Nonlinear Frequency-Domain Analysis of Unsteady Flows in Turbomachinery with Multiple Excitation Frequencies. AIAA Paper 2006-2995.

[16] Giles, M. B., 1990. "Non-Reflecting Boundary Conditions for Euler Equation Calculations". *AIAA Journal*, ***28***(12), Dec., pp. 2050–2058.

[17] Hall, K. C., Lorence, C. B., and Clark, W. S., 1993. Nonreflecting Boundary Conditions for Linearized Aerodynamic Calculations. AIAA Paper 93-0882.

[18] Saxer, A. P., 1992. "A Numerical Analysis of Three-Dimensional Inviscid Rotor/Stator Interactions Using Non-Reflecting Boundary Conditions". PhD thesis, MIT, Cambridge, MA.

[19] Weiss, J. M., Maruszewski, J. P., and Smith, W. A., 1999. "Implicit Solution of Preconditioned Navier-Stokes Equations Using Algebraic Multigrid". *AIAA Journal*, ***37***(1), Jan., pp. 29–36.

[20] Ekici, K., and Hall, K. C., 2007. "Nonlinear Analysis of Unsteady Flows in Multistage Turbomachines Using Harmonic Balance". *AIAA Journal*, ***45***(5), May, pp. 1047–1057.

Copyright © 2011 by ASME